ACS APPLIED NANO MATERIALS

www.acsanm.org Article

Large-Area Monolayer MoS_2 Nanosheets on GaN Substrates for Light-Emitting Diodes and Valley-Spin Electronic Devices

Peng Yang,[¶] Haifeng Yang,[¶] Zhengyuan Wu, Fuyou Liao, Xiaojiao Guo, Jianan Deng, Qiang Xu, Haomin Wang, Junjie Sun, Fei Chen, Wenzhong Bao, Laigui Hu, Zhongkai Liu, Yulin Chen, Zhi-Jun Qiu, Zhilai Fang, Ran Liu,* and Chunxiao Cong*

Cite This: *ACS Appl. Nano Mater.* 2021, 4, 12127−12136 Read Online

ACCESS | Metrics & More | Article Recommendations | Supporting Information

ABSTRACT: Van der Waals heterostructures composed of atomically thin two-dimensional (2D) materials and three-dimensional (3D) materials provide a multidimensional material integration strategy, which combines materials with different characteristics leading to a wider degree of freedom than a single component, and offer a way for developing electronic and optoelectronic devices with multifunctionalities, such as high-frequency electronic devices, photodetectors, valley-spin electronic devices, and so on. This report demonstrates the direct growth of large-area monolayer MoS_2 single-crystal nanosheets with a side length of more than 100 μm on 3D GaN substrates by the perylene-3,4,9,10-tetracarboxylic acid tetrapotassium salt (PTAS) seed-assisted chemical vapor deposition (CVD) method. The seeding promoters changed the growth kinetics of MoS_2 on the GaN substrate, which is different from the previously reported epitaxial growth behavior. The size of our synthesized single-crystal MoS_2 nanosheets is 2 orders of magnitude larger than the reported epitaxially grown MoS_2 on the GaN substrate. Meanwhile, the as-synthesized MoS_2 by the seed-assisted CVD method has comparable crystal quality as that of the reported epitaxially grown MoS_2 on the GaN substrate. Moreover, detailed characterizations indicate that noticeable charge transfer occurs between MoS_2 and the GaN substrate, which suggests that the MoS_2/GaN heterostructure has great potential applications in the field of light-emitting diodes (LED) and valley-spin electronic devices.

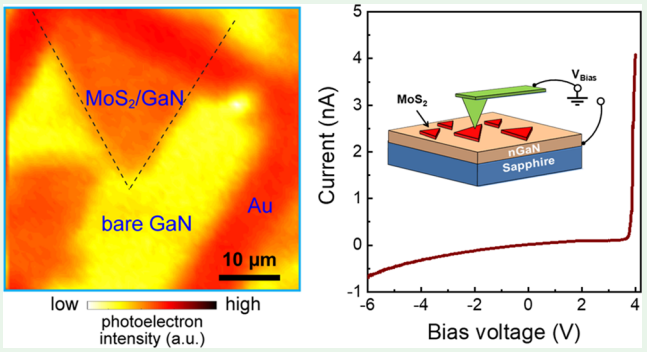

KEYWORDS: *MoS_2, chemical vapor deposition, seeding promoters, 2D/3D heterostructures, charge transfer*

INTRODUCTION

In recent years, van der Waals heterostructures composed of newly emerged two-dimensional (2D) materials and traditional three-dimensional (3D) materials have attracted extensive attention.[1−6] The coupling of quasi-particles at the interface of heterostructures provides a new route for developing innovative device designs such as tunnel diodes, ultrabroadband photodetectors, light-emitting diodes (LEDs), and high-power devices.[7−13] As a typical III−V compound, GaN is known as a third-generation semiconductor after silicon and gallium arsenide. The crystal structure of GaN is a hexagonal wurtzite configuration, as the inner Ga and N atoms are all covalently bonded with each other, which is similar to silicon and diamond materials. Therefore, GaN can be considered a typical 3D material. Also, GaN is a wide direct-band-gap semiconductor with a bandgap of 3.4 eV, which is widely used in high-power devices, advanced wireless communication, and high-frequency microwave devices.[14,15] Good chemical stability at high temperatures and compatibility with mature process semiconductor technology make GaN a potential substrate to grow 2D semiconductor materials and construct 2D/3D heterostructures, meeting the demands of new electronic devices with multifunctionality and further broadening the application fields of both 2D materials and 3D GaN.[9−12] Monolayer MoS_2 is a typical 2D semiconductor that has been intensively studied in the past decade. Both GaN and MoS_2 belong to the hexagonal crystal system with similar lattice constants (3.19 Å for GaN, 3.16 Å for MoS_2); the in-plane lattice mismatch is less than 1%. Furthermore, the thermal expansion coefficients of GaN and MoS_2 are very close (3.95×10^{-6} K^{-1} for GaN, 4.92×10^{-6} K^{-1} for MoS_2).[16−18] Thus, we can anticipate that the direct growth of MoS_2 on the GaN substrate will not generate in-plane stress during the growth process, which can guarantee the high crystal quality of MoS_2.

Received: August 25, 2021
Accepted: October 27, 2021
Published: November 9, 2021

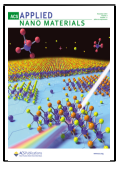

https://doi.org/10.1021/acsanm.1c02662
ACS Appl. Nano Mater. 2021, 4, 12127−12136

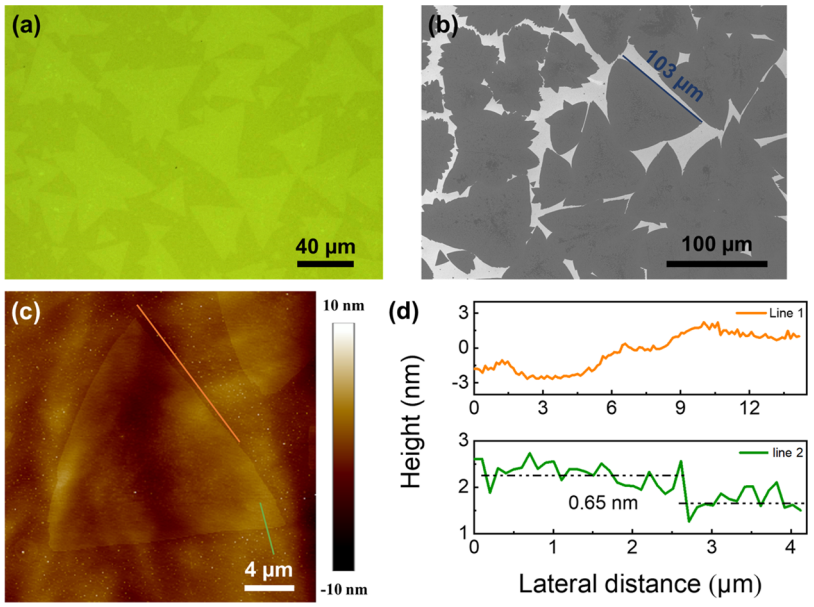

Figure 1. (a, b) Optical and SEM images of MoS_2 grown on GaN(0001)/sapphire substrates. (c) AFM image of the MoS_2/GaN heterostructure. (d) Height profile corresponding to the same color line marked in (c).

There are some interesting phenomena in the hybrid structure composed of the 3D GaN and the 2D MoS_2, such as the increased polarization of MoS_2 under circularly polarized light and the band bending at the interface of the heterostructures.[11,19] At present, a transfer method was used to prepare 2D/3D heterostructures. For example, Moun et al. transferred the mechanically exfoliated MoS_2 to the GaN substrates and studied the photodetection and diode characteristics of the MoS_2/GaN heterostructure.[20] However, the exfoliated MoS_2 sample is not suitable for the preparation of large-scale integrated devices. Henck et al. transferred large-area chemical vapor deposition (CVD)-grown MoS_2 nanoflakes onto GaN substrates via the poly(methyl methacrylate) (PMMA)-assisted method. They found a significant charge-transfer phenomenon at the interface of the MoS_2/GaN heterostructure, whereas the wetting transfer method can cause damage to the crystal quality of MoS_2 during the chemical corrosion period and introduce some unwanted residual impurities.[19] The CVD method has unique advantages in the preparation of large-area 2D/3D heterostructures due to its benefits of good controllability, relatively low cost, and good crystallinity of the obtained thin film. It is the most popular preparation technology currently for large-area 2D materials and their complex heterostructures.[21−27] Ruzmetov and Wan et al. reported that CVD-grown MoS_2 nanosheets on GaN substrates exhibited apparent epitaxial growth behavior; the MoS_2 domains were aligned at either 0 or 60° orientations.[9−11] However, the side length of the MoS_2 nanosheets obtained was generally below 10 μm, which limits its application in the field of large-scale devices.[9]

To overcome the bottleneck of size limit in CVD growth of monolayer MoS_2 epitaxially grown on traditional 3D GaN substrates, we used perylene-3,4,9,10-tetracarboxylic acid tetrapotassium salt (PTAS) seeds to promote CVD growth of large-area monolayer MoS_2 single crystals on GaN substrates. A triangle-shaped monolayer MoS_2 single-crystal nanosheet with a side length of more than 100 μm was synthesized on GaN substrates, which is 2 orders of magnitude larger than the size of MoS_2 crystal domains epitaxially grown on the GaN substrates reported in the literature.[9−11] Since the introduced PTAS catalyst changed the surface energy of the GaN growth substrate, the MoS_2 nanosheets do not exhibit epitaxial growth behavior on the substrate, that is, the MoS_2 nanosheets have no specific orientation with GaN substrates. A series of characterizations were conducted on the performance of the MoS_2/GaN heterostructure, including Raman spectroscopy, photoluminescence spectroscopy (PL), X-ray photoelectron spectroscopy (XPS), angle-resolved photoemission spectroscopy with submicron lateral resolution (micro-ARPES), Kelvin probe force microscopy (KPFM), and conductive atomic force microscopy (CAFM). The results indicate that the MoS_2 grown on GaN substrates has a good crystal quality, and there is a significant charge transfer between MoS_2 and GaN. The performance of our synthesized large-area MoS_2/GaN is comparable to that of the epitaxially grown MoS_2/GaN heterostructures. The direct growth of MoS_2/GaN heterostructures introduced in this paper promotes the large-scale preparation of 2D/3D heterostructures and their application in the field of optoelectronic devices.

EXPERIMENTAL SECTION

Growth of MoS_2. The MoS_2 sample was grown by the CVD method on n-type GaN(0001)/sapphire substrates in a two-temperature-zone furnace. The GaN(0001) film was epitaxially grown on Al_2O_3 with dislocation density less than 5×10^8 cm^{-2} and a thickness of 4.5 μm. Before growth of MoS_2, the GaN(0001)/sapphire substrates were pretreated by drop-casting 5 μL of 100 μM PTAS. Then, 150 mg of sulfur (Aladdin, 99.99%) and 3 mg of MoO_3 (Aladdin, 99.9%) were used as the growth precursors, and high-purity N_2 gas (99.999%) was used as the carrier gas. The two zones were separately heated to 170 and 680 °C within 38 min and maintained for 3 min for the growth with 20 sccm N_2 flow in an atmospheric pressure.

Characterization. The detailed morphologies of MoS_2 were characterized by optical microscopy (Keyence digital microscope VHX-600), scanning electron microscopy (SEM) (Zeiss Sigma HD), and atomic force microscope (AFM) (Bruker, Dimension FastScan) equipped with CAFM and KPFM test modules. The Raman and PL

https://doi.org/10.1021/acsanm.1c02662
ACS Appl. Nano Mater. 2021, 4, 12127−12136

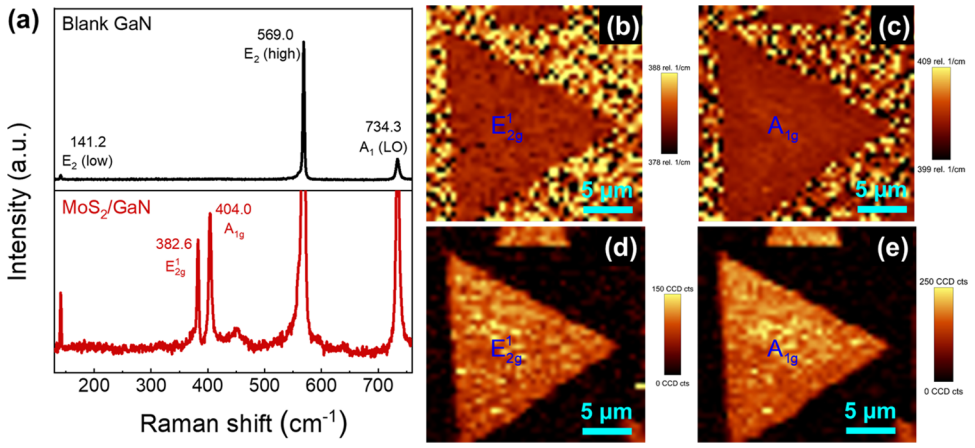

Figure 2. (a) Raman spectrum of blank GaN and MoS_2/GaN heterostructures. (b, c) Raman mapping of peak positions of E^1_{2g} mode (b) and A_{1g} mode (c). (d, e) Raman mapping of peak intensities of E^1_{2g} mode (d) and A_{1g} mode (e).

spectra were performed by WITec Alpha 300R with 532 or 633 nm laser. The laser power of 3 mW was chosen to obtain a Raman spectrum with a good signal-to-noise ratio. The XPS measurement was carried out by ThermoFisher ESCALAB 250Xi with an Al Kα X-ray source. The electrodes were patterned by photolithography using a laser direct writing machine (Microwriter ML3) followed by deposition of 5 nm of Cr and 50 nm of Au. Micro-ARPES measurements were conducted at the SpectroMicroscopy beamline at the Elettra Synchrotron Light Source (Italy) utilizing a 74 eV photon beam.[28] The measurement temperature was 100 K. The overall energy, angle, and lateral resolutions were 50 meV, 1, and ~1 μm, respectively. Au mesh grids (40 × 40 μm^2) were deposited on MoS_2/GaN by the laser direct writing machine and the lithography technology to avoid the charging effect in photoemission. Prior to ARPES measurements, MoS_2/GaN heterostructures were annealed at 573 K in a preparation chamber.

RESULTS AND DISCUSSION

The growth of 2D monolayer MoS_2 nanosheets in our experiment was conducted by the CVD method on 3D GaN substrates with special temperature control of the growth source as described in the Experimental Section. Figure 1a,b shows the morphology of MoS_2 grown on a GaN(0001)/sapphire substrate assisted-growth by PTAS seeding promoters under an optical microscope and SEM. It was found that the orientation of these MoS_2 domains is randomly distributed, and the maximum side length of triangular-shaped MoS_2 domains can reach up to 103 μm, which is 2 orders of magnitude larger than the MoS_2 domains epitaxially grown on the GaN substrate with a specific orientation by the CVD method in previous reports.[9−11] This can be ascribed to the fact that the introduced seeds changed the surface energy of the GaN substrate and reduced the nucleation energy of MoS_2 during the growth period,[29−31] making the growth of MoS_2 on GaN from thermodynamic equilibrium control with specific orientation become kinetic rate control with a random direction.[32] Our growth strategy for the synthesis of MoS_2 single crystals with a side length of up to tens to hundreds of microns on GaN substrates has a lower growth temperature at 680 °C and a shorter growth time for 3 min compared with the epitaxial growth of MoS_2 on GaN at 800 °C for 15 min with side length less than 10 μm without seeding promoters as reported in the literature.[9] The growth mechanism may be described as follows. Under the growth temperature of MoS_2, the PTAS seeds decompose into small fragments, which contain conjugate benzene rings as the parent molecule. The plane structure of conjugate benzene rings can be absorbed on the surface of the GaN substrates and thus change the surface energy of GaN. At the same time, the conjugate benzene rings can also be highly reactive centers, which can anchor the growth source, that is, Mo and S atoms, in a plane and finally form a nucleation center, followed by the extended growth of MoS_2 in a planar way. With prolonged growth time, we can obtain a continuous monolayer MoS_2 film as seen in the following device sections. Further analysis of the morphology of MoS_2/GaN by AFM indicates that MoS_2 is a monolayer with a thickness of 0.65 nm, which is consistent with the thickness of the monolayer MoS_2 grown by CVD and the mechanical exfoliated sample.[31,33] From the AFM morphology image, it can be seen that the surface of the MoS_2 flake is very clean and there are almost no impurity particles. On the other hand, we find that there are only a few incompletely reacted MoO_x molybdenum source particles in the blank GaN area as will be discussed by the XPS results below. Although the fluctuation of GaN topography exceeds 5 nm, the as-grown monolayer MoS_2 domains closely attach to the GaN surface. In view of the good chemical stability of GaN at high temperatures, GaN can also be a suitable substrate for growing other 2D transition-metal dichalcogenide (TMDC) compounds, thereby constructing various 2D/3D heterojunctions with more abundant properties.

The composition and crystal quality of the MoS_2/GaN heterostructure were studied with Raman spectroscopy. In general, Raman spectroscopy is a useful characterization tool that can quickly and nondestructively analyze the layer number and crystal quality of 2D materials.[34,35] Figure 2 shows the Raman spectrum and mapping results of the MoS_2/GaN heterostructure. The upper panel of Figure 2a is the Raman spectrum of the blank GaN substrate after growing MoS_2. There are three typical Raman peaks located at 141.2 cm^{-1} (E_2, low), 569.0 cm^{-1} (E_2, high), and 734.3 cm^{-1} A_1 (LO), consistent with the Raman features of GaN with a hexagonal wurtzite configuration as reported in the literature,[36,37] indicating that the GaN substrate can be stable under the high-temperature growth environment of MoS_2. The lower panel of Figure 2a is the Raman spectrum of the MoS_2/GaN heterostructure. In addition to the Raman peaks of GaN, two other typical Raman peaks of MoS_2 can be detected at 382.6 cm^{-1} and 404.0 cm^{-1}, which belong to the in-plane vibration mode (E^1_{2g}) and the out-of-plane vibration mode (A_{1g}),

https://doi.org/10.1021/acsanm.1c02662
ACS Appl. Nano Mater. 2021, 4, 12127−12136

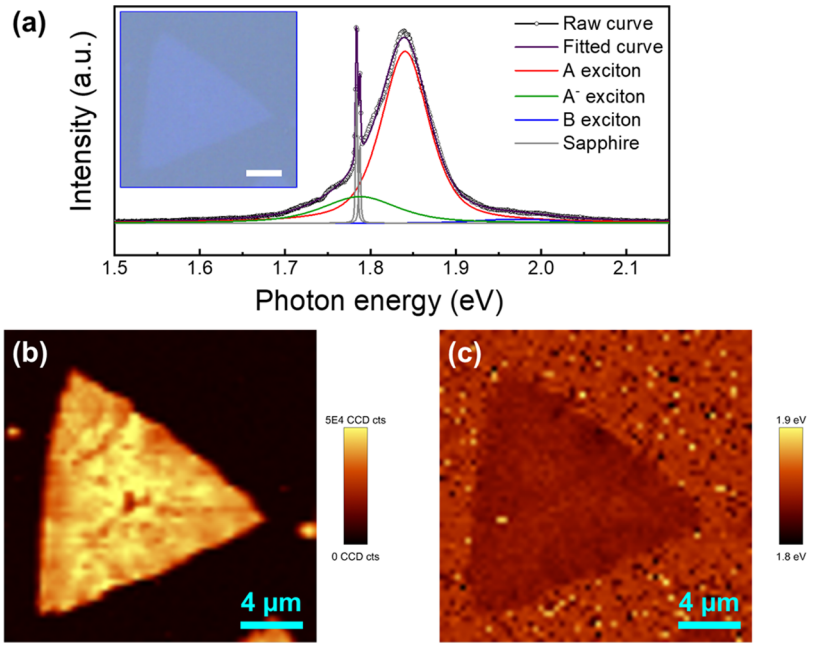

Figure 3. (a) PL spectrum of the monolayer MoS_2 domain grown on GaN; the inset is the optical image of the MoS_2/GaN heterostructure. The scale bar is 4 μm. (b, c) PL intensity mapping (b) and peak position mapping (c) of a typical monolayer MoS_2 domain on GaN corresponding to the inset in (a).

respectively. The difference between these two peaks is 21.4 cm^{-1}, which is slightly larger than that of the monolayer MoS_2 grown on SiO_2/Si wafers and sapphire substrates by CVD.[29−31] Such a peak difference may be due to the thermal effect caused by the detection laser with a power of 3 mW.[38,39] On the other hand, it may be caused by the charge transfer between MoS_2 and the GaN substrates, thus changing the doping level of MoS_2 as the peak position of the A_{1g} vibration mode is sensitive to doping.[40] Figure 2b,c shows the Raman mapping of the peak position of the two vibration modes (E^1_{2g} and A_{1g}) of a typical MoS_2 domain. The peak positions of the two Raman modes have almost no change in the entire MoS_2 area, indicating that there is no local stress and local doping within the MoS_2 domain. Figure 2d,e shows the Raman mapping of the intensity of E^1_{2g} and A_{1g} modes; the spatially uniform intensity of these two Raman modes indicates that the quality of the CVD-grown MoS_2 nanosheet on the GaN substrate is of good uniformity.

Then, we used PL spectroscopy to further evaluate the quality of the MoS_2 grown on the GaN substrate. Figure 3 shows the PL spectrum and mapping of the MoS_2/GaN heterostructure. Since monolayer MoS_2 is a direct-band-gap semiconductor, a strong PL peak is detected under 532 nm laser radiation, as shown in Figure 3a. The PL spectrum was fitted for better understanding the behavior of exciton in MoS_2; the peak located at 1.84 eV corresponds to the A exciton peak in MoS_2. The full width at half-maximum (FWHM) of A exciton is only 66 meV; such a narrow peak width indicates the high quality of the MoS_2 grown on GaN. The sharp peaks near 1.8 eV indicate the sapphire substrate. Due to the lack of inversion symmetry and the strong spin−orbital coupling effect in the monolayer MoS_2, leading to the splitting of the valence-band maximum,[41] there are two direct exciton emission peaks, that is, A exciton and B exciton, as shown in the PL spectrum of MoS_2, but the B exciton peak is very weak. Recently, it has been reported that the intensity ratio of A exciton versus B exciton (A/B) can be used to evaluate the crystal quality of MoS_2 qualitatively. The larger the ratio of A/B, the better the quality of MoS_2.[42,43] The PL spectral shape of our synthesized MoS_2 on the GaN substrate is very similar to the suspended monolayer MoS_2 and the CVD-grown MoS_2 sample on h-BN,[44,45] indicating that much less defects exist in MoS_2 samples, further illustrating the excellent quality of the MoS_2 grown on the GaN substrate. Figure 3b,c shows the PL mapping of the peak intensity and the peak position of the monolayer MoS_2 domain on the GaN substrate. It is also found that the peak intensity and the peak position of the entire crystal domain are relatively uniform, indicating that the quality of the MoS_2 crystal domain is uniform. However, the very small area with a darker intensity in the center of the mapping image can be due to the initial nucleation point of MoS_2.[46] The above optical properties further suggest that MoS_2 grown on GaN has a good crystal quality, which may benefit from the minor lattice mismatch ratio of MoS_2 and the GaN substrate, making GaN an excellent substrate for growing other high-quality 2D TMDC compounds that are lattice-matched with GaN. In addition, the circular polarization behavior of the MoS_2/GaN heterostructure is also studied. Figure S1a shows the circularly polarized PL spectrum of the MoS_2/GaN heterostructure under a 633 nm laser ($h\nu$ = 1.96 eV) at room temperature. The use of an excitation wavelength of 633 nm here is due to the fact that resonant excitation can increase the polarization of 2D semiconductor materials under helicity circularly polarized laser because of the suppressed phonon-assisted intervalley scattering.[11] The following formula can calculate the polarization helicity

$$P = (I_{\sigma^+} - I_{\sigma^-})/(I_{\sigma^+} + I_{\sigma^-}) \quad (1)$$

where I_{σ^+} and I_{σ^-} are the intensities of the PL spectra of MoS_2 under right-circularly and left-circularly light. It is found that MoS_2 on the GaN substrate has obvious valley polarization at

https://doi.org/10.1021/acsanm.1c02662
ACS Appl. Nano Mater. 2021, 4, 12127−12136

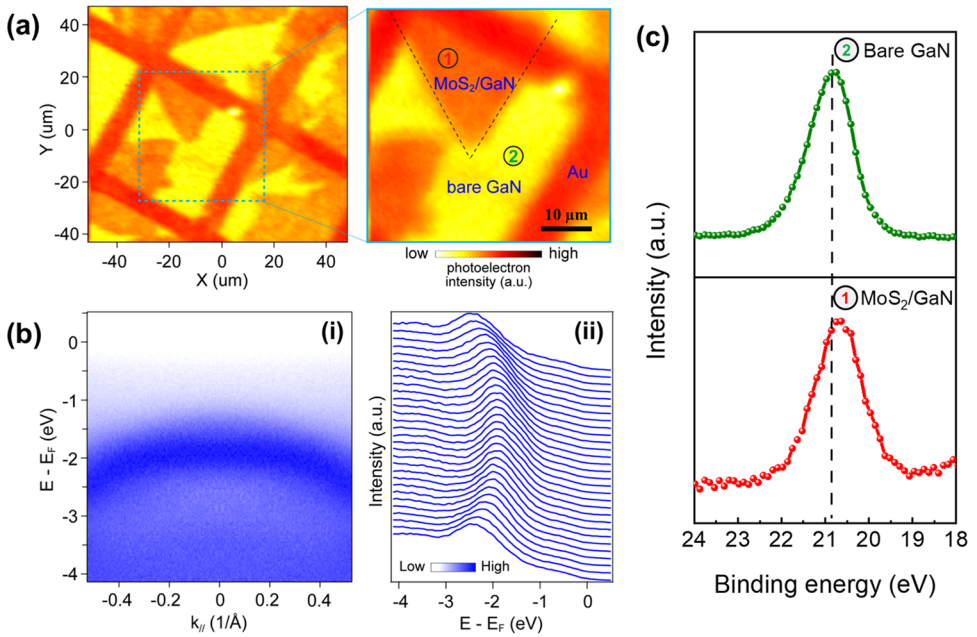

Figure 4. (a) Micro-ARPES photoemission real-space map of MoS_2/GaN measured with the photon energy of 74 eV. Photoelectrons with approximately the maximum kinetic energy are integrated. Regions of MoS_2/GaN, bare GaN, and Au mesh are marked. (b) ARPES photoemission spectra of the MoS_2/GaN heterostructure near the Γ point of the Brillouin zone (i) and its momentum−distribution curve plots (ii), both of which clearly show good holelike band dispersions of the valence band. (c) High-resolution photoelectron spectrum of the Ga 3d core-level electrons on bare GaN and MoS_2/GaN heterostructures corresponding to the marked dot in (a).

room temperature, which is much larger than that of MoS_2 grown on the sapphire substrate in the same condition as shown in Figure S1b, indicating that the interaction between the GaN substrate and MoS_2 can manipulate the valley helicity of MoS_2, which is due to the competition between the intervalley scattering rate and the faster exciton decay rate in MoS_2 caused by the GaN substrate.[11] The charge transfer in the interface of the MoS_2/GaN heterostructure increases the circular polarization of MoS_2, making the 2D/3D heterostructures composed of TMDCs and GaN have great promising application prospects in the field of valley electronics.

The composition of the MoS_2/GaN heterostructure was further analyzed by XPS as it is an important characterization technique for qualitative and quantitative analyses of the element component in samples. As shown in Figure S2a, the Mo 3d core-level spectra can be fitted with two pair peaks. The Mo $3d_{3/2}$ and $3d_{5/2}$ with band energies of 235.6 and 232.4 eV correspond to the incompletely reacted MoO_x particles as mentioned above measured on blank GaN by AFM. The other pair peaks of $3d_{3/2}$ at 232.6 eV and $3d_{5/2}$ at 229.5 eV correspond to Mo^{4+} in MoS_2. The spin−orbit splitting energy of Mo^{4+} 3d is 3.1 eV. These binding energies of Mo and S are consistent with the reported XPS peak values of MoS_2 in the literature.[47] At the same time, we also measured the XPS spectra of the Ga 3s core level as shown in Figure S2b, which is in line with the Ga 3s of GaN reported in the literature,[48] further indicating that GaN can be stable in the growth environment of MoS_2.

To investigate the band structure and electronic properties of the 2D/3D hybrid MoS_2/GaN heterostructure, we carried out state-of-the-art micro-ARPES measurements.[28,49,50] After focusing the light to submicron size, we scanned the sample surface and acquired the photoemission 2D real-space map at the submicron lateral resolution as shown in Figure 4a, in which regions of the triangle-shaped MoS_2/GaN heterostructure, bare GaN, and Au mesh can be apparently discerned. Then, we moved the light beam to the MoS_2/GaN heterostructure region and obtained the valence-band dispersion of MoS_2 at the Γ point of the Brillouin zone. Clearly, the valence band exhibits good holelike dispersions,[19] as shown by the false-color display of the ARPES spectrum in Figure 4b(i) and massive plots of momentum−distribution curves in Figure 4b(ii). We note that the quality of our ARPES data is comparable to that measured on exfoliated MoS_2 nanoflakes.[51,52] Interestingly, from the high-resolution photoelectron spectrum of the Ga 3d core-level electrons in the MoS_2/GaN heterostructure as shown in Figure 4c, we found that Ga 3d has 200 meV red-shifted in the MoS_2/GaN heterostructure compared to the blank GaN substrate. This shift at a lower binding energy suggests that band bending occurs at the interface of the heterostructure as a result of charge transfer from the 2D monolayer MoS_2 to GaN.[19]

To explain the charge-transfer phenomenon at the MoS_2/GaN interface, KPFM was used to characterize the surface potential mapping of the MoS_2/GaN heterostructure as shown in Figure S3. There is a significant potential difference between the MoS_2 domain and GaN, and the potential distribution is uniform throughout the whole MoS_2 domain. The contact potential difference (CPD) between the KPFM tip and the sample is given by

$$(\mathrm{CPD})_{\mathrm{MoS_2}} = \frac{\phi_{\mathrm{tip}} - \phi_{\mathrm{MoS_2}}}{-e} \quad \text{and} \quad (\mathrm{CPD})_{\mathrm{GaN}} = \frac{\phi_{\mathrm{tip}} - \phi_{\mathrm{GaN}}}{-e} \tag{2}$$

where ϕ_{tip}, ϕ_{GaN}, and $\phi M_{\mathrm{oS_2}}$ are the work functions of the KPFM tip, GaN, and MoS_2, respectively. The CPD between MoS_2 and GaN is given by

https://doi.org/10.1021/acsanm.1c02662
ACS Appl. Nano Mater. 2021, 4, 12127−12136

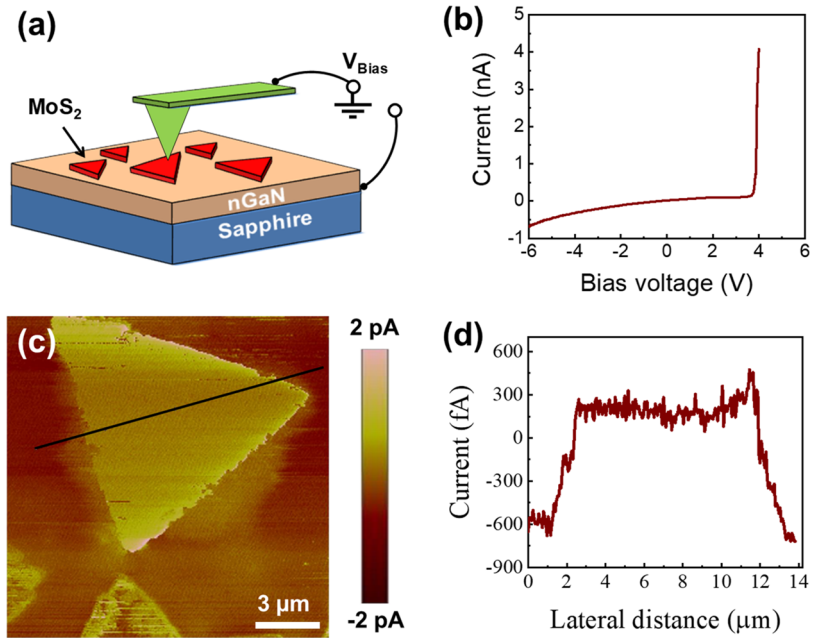

Figure 5. (a) Schematic of CAFM measurement of the MoS_2/GaN heterostructure. (b) $I-V$ measurement of MoS_2/GaN by CAFM. (c) Current mapping of a typical MoS_2 domain on GaN. (d) Current difference with lateral distance across the MoS_2/GaN heterostructure corresponding to the dark line marked in (c).

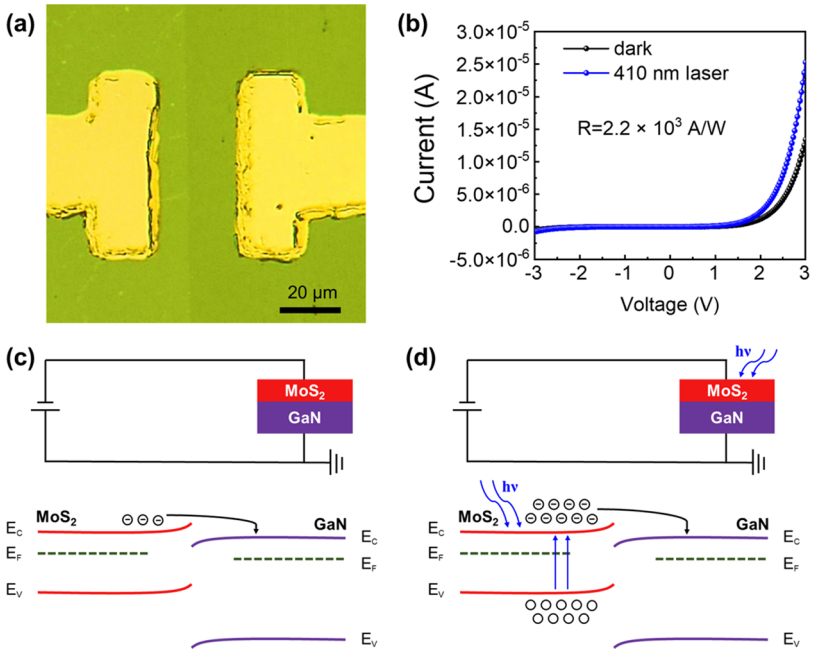

Figure 6. (a) Optical image of the continuous film of the MoS_2/GaN heterostructure device. (b) Current−voltage ($I-V$) curve of the MoS_2/GaN photodetector under dark conditions and after being illuminated by a 410 nm laser. (c, d) Band alignment of the MoS_2/GaN heterostructure before (c) and after illumination (d) under a positive bias voltage given to GaN with respect to MoS_2.

$$\Delta(\mathrm{CPD}) = (\mathrm{CPD})_{\mathrm{GaN}} - (\mathrm{CPD})_{\mathrm{MoS_2}} = \frac{\phi_{\mathrm{MoS_2}} - \phi_{\mathrm{GaN}}}{-e} \quad (3)$$

It can be seen from Figure S3b that the surface potential of the GaN substrate is about 55 mV higher than that of the monolayer MoS_2, so the work function of the GaN substrate is 55 meV larger than that of the MoS_2 flake. Therefore, MoS_2 forms a heterojunction with the GaN substrate and has a built-in potential difference, indicating that a significant charge transfer occurs at the interface between the two materials.[20]

The charge transport at the vertical 2D/3D heterojunction interface is closely related to the properties of the 2D material. The current−voltage ($I-V$) relationship of the MoS_2/GaN heterojunction was carried out by CAFM, as illustrated by Figure 5a. The CAFM tip is contacted with the top surface of the MoS_2, and the other electrode is connected with blank GaN. The $I-V$ measurement results in Figure 5b show that the current can vertically flow through the van der Waals gap at the

https://doi.org/10.1021/acsanm.1c02662
ACS Appl. Nano Mater. 2021, 4, 12127−12136

interface of the MoS_2/GaN heterojunction, resulting in obvious rectification characteristics, allowing the MoS_2/GaN heterostructure to be applied to the light-emitting diode. The current conduction through vertically stacked 2D/3D semiconductor heterojunctions brings the possibility of complex structures with specific electrical characteristics, such as utilizing MoS_2 as the epitaxial center for the growth of other 2D materials. It can be seen from Figure 5c,d that the electrical conductivity of the entire MoS_2 domain region in the MoS_2/GaN heterojunction is significantly larger than that of the blank GaN substrate, which is consistent with the results reported in the literature.[9]

Since MoS_2 can absorb visible light and generate photogenerated carriers, this 2D/3D heterojunction can be further applied to photodetectors. As shown in Figure 6a,b, the $I-V$ curves present a rectifying behavior, which can be explained by the built-in potential between MoS_2 and GaN indicated by the KPFM results. Since the Fermi level of GaN is at a lower energy level than that of MoS_2, the built-in electric field is directed from MoS_2 to GaN. The band alignment under bias voltage was illustrated based on the KPFM analysis, as shown in Figure 6c.[20,53,54] When a positive voltage is applied to GaN with respect to MoS_2, the built-in potential will be offset, leading to a decrease in the effective barrier and more electrons can transport from MoS_2 to GaN, resulting in a high value of the current. Similarly, a low value of the current is observed owing to the reinforcing of the built-in potential when reverse-biased. The photoresponse of the MoS_2/GaN heterostructure is illustrated by illuminating the device by a 410 nm laser as the energy is located between the bandgap of MoS_2 and GaN with a power density of 1 mW/cm^2; the photoresponsivity (R) can illustrate the figure-of-merit of a photodetector by the following equation

$$R = \frac{I_{\text{illuminated}} - I_{\text{dark}}}{P_{\text{illuminated}}} \tag{4}$$

where $I_{\text{illuminated}}$, I_{dark}, and $P_{\text{illuminated}}$ are the current after illumination, dark current, and the illuminated power of laser light falling on the active area of the device, respectively. The current was enhanced upon irradiation, which can be due to the increase of photogenerated carriers transferred from MoS_2 to GaN under a bias voltage. The calculated R of the MoS_2/GaN heterostructure is 2.2×10^3 A/W at the bias voltage of 3 V; this value is higher than that of photodetectors based on monolayer MoS_2 field-effect transistors (FETs),[55] which might have contributed to the traps induced by the interface of the heterostructure. When the photogenerated holes are captured by the traps, hindering the recombination of excitons, then electrons are extracted from the source to maintain the charge neutrality of the channel, resulting in an ultrahigh photoresponsivity. However, the value of photoresponsivity is a little lower than the multilayer MoS_2/GaN heterostructure due to the stronger absorption in multilayer MoS_2 samples.[20,54] We further analyze the external quantum efficiency (EQE) of the MoS_2/GaN heterostructure-based photodetector, which refers to the photoconversion efficiency, and can be expressed by the following formula

$$\text{EQE} = \frac{h \times c \times R}{e \times \lambda} \tag{5}$$

where h is the Planck constant, c is the speed of light, R is the photoresponsibility as calculated based on eq 4, e is the charge of the electron, and λ is the wavelength of the illumination laser.[54] The EQE is calculated to be 6.6×10^5% at the bias voltage of 3 V. A comparison of the performance parameters of the MoS_2/GaN photodetector with previous reports is outlined in Table S1,[20,53−56] which means that the MoS_2/GaN heterostructure shows potential application prospects in photodetectors.

CONCLUSIONS

In summary, we demonstrated the utilizing of the PTAS seeding promoter-assisted CVD method to synthesize large-area monolayer MoS_2 single-crystal nanosheets with side length more than 100 μm on GaN substrates, which is 2 orders of magnitude larger than the reported epitaxially grown MoS_2 nanosheets on GaN substrates. The introduction of the PTAS seeds changed the surface energy of the GaN substrate and promoted the nucleation and rapid growth of MoS_2. A series of characterization results indicate that the seed-assisted CVD-grown large-area monolayer MoS_2 nanosheets on GaN have a good crystal quality. Their quality is comparable to the reported monolayer MoS_2 epitaxially grown on GaN. Our work provides a valuable guide for the large-area growth of 2D/3D heterostructures and their applications in LED, valley-spin electronic devices, and photodetectors, which are helpful for electrical designers and fundamental research in multifunctional devices.

ASSOCIATED CONTENT

Supporting Information

The Supporting Information is available free of charge at https://pubs.acs.org/doi/10.1021/acsanm.1c02662.

Circularly polarized PL characterizations of MoS_2 on GaN and on sapphire substrates, elemental analysis of the MoS_2/GaN heterostructure by XPS, surface potential distribution of MoS_2/GaN by KPFM, and photoresponse of the MoS_2/GaN heterostructure-based device (PDF)

AUTHOR INFORMATION

Corresponding Authors

Ran Liu − *State Key Laboratory of ASIC and System, School of Information Science and Technology, Fudan University, Shanghai 200433, China*; Email: rliu@fudan.edu.cn

Chunxiao Cong − *State Key Laboratory of ASIC and System, School of Information Science and Technology, Fudan University, Shanghai 200433, China; Yiwu Research Institute of Fudan University, Yiwu City 322000 Zhejiang, China; Academy for Engineering and Technology, Fudan University, Shanghai 200433, China*; orcid.org/0000-0001-9786-825X; Email: cxcong@fudan.edu.cn

Authors

Peng Yang − *State Key Laboratory of ASIC and System, School of Information Science and Technology, Fudan University, Shanghai 200433, China; Yiwu Research Institute of Fudan University, Yiwu City 322000 Zhejiang, China*

Haifeng Yang − *School of Physical Science and Technology, ShanghaiTech University, 201210 Shanghai, China*

Zhengyuan Wu − *School of Information Science and Technology, and Academy for Engineering and Technology, Fudan University, Shanghai 200433, China*; orcid.org/0000-0003-0345-8423

https://doi.org/10.1021/acsanm.1c02662
ACS Appl. Nano Mater. 2021, 4, 12127−12136

Fuyou Liao − *State Key Laboratory of ASIC and System, School of Microelectronics, Fudan University, Shanghai 200433, China*
Xiaojiao Guo − *State Key Laboratory of ASIC and System, School of Microelectronics, Fudan University, Shanghai 200433, China*
Jianan Deng − *State Key Laboratory of ASIC and System, School of Information Science and Technology, Fudan University, Shanghai 200433, China*
Qiang Xu − *University of Michigan—Shanghai Jiao Tong University Joint Institute, Shanghai Jiao Tong University, Shanghai 200240, China*
Haomin Wang − *State Key Laboratory of Functional Materials for Informatics, Shanghai Institute of Microsystem and Information Technology, Chinese Academy of Sciences, Shanghai 200050, China*
Junjie Sun − *State Key Laboratory of Laser Interaction with Matter, Innovation Laboratory of Electro-Optical Countermeasures Technology, Changchun Institute of Optics, Fine Mechanics and Physics, Chinese Academy of Sciences, Changchun, Jilin 130033, China*
Fei Chen − *State Key Laboratory of Laser Interaction with Matter, Innovation Laboratory of Electro-Optical Countermeasures Technology, Changchun Institute of Optics, Fine Mechanics and Physics, Chinese Academy of Sciences, Changchun, Jilin 130033, China*
Wenzhong Bao − *State Key Laboratory of ASIC and System, School of Microelectronics, Fudan University, Shanghai 200433, China*
Laigui Hu − *State Key Laboratory of ASIC and System, School of Information Science and Technology, Fudan University, Shanghai 200433, China;* orcid.org/0000-0003-1995-1423
Zhongkai Liu − *School of Physical Science and Technology, ShanghaiTech University, 201210 Shanghai, China*
Yulin Chen − *School of Physical Science and Technology, ShanghaiTech University, 201210 Shanghai, China*
Zhi-Jun Qiu − *State Key Laboratory of ASIC and System, School of Information Science and Technology, Fudan University, Shanghai 200433, China*
Zhilai Fang − *School of Information Science and Technology, and Academy for Engineering and Technology, Fudan University, Shanghai 200433, China*

Complete contact information is available at: https://pubs.acs.org/10.1021/acsanm.1c02662

Author Contributions

[¶]P.Y. and H.Y. contributed equally to this work.

Author Contributions

C.C. and R.L. directed the research work. C.C. and P.Y. conceived and designed the experiments. P.Y. fabricated the MoS_2/GaN samples and performed the Raman and PL measurements. H.Y. conducted the ARPES test. P.Y., F.L., and X.G. fabricated the devices and performed the electrical performance measurements. P.Y. and Q.X. performed AFM, KPFM, and CAFM characterizations. C.C., P.Y., H.Y., H.W., and Z.-J.Q. analyzed the data. C.C., P.Y., and H.Y. cowrote the manuscript. All authors discussed the results and commented on the manuscript.

Notes

The authors declare no competing financial interest.

■ ACKNOWLEDGMENTS

This work was supported by the National Key R&D Program of China (Grant No. 2018YFA0703700), the National Natural Science Foundation of China (Grant No. 61774040, 61774042, and 12004248), the Shanghai Municipal Science and Technology Commission (Grant No. 18JC1410300), the Shanghai Municipal Natural Science Foundation (Grant No. 20ZR1403200), the Shanghai Sailing Program (No. 20YF1430500), the Fudan University-CIOMP Joint Fund (Grant No. FC2018-002), the National Young 1000 Talent Plan of China, the "First-Class Construction" project of Fudan University (No. XM03170477), and the State Key Laboratory of ASIC & System, Fudan University (No. 2018MS001).

■ REFERENCES

(1) Liu, Y.; Huang, Y.; Duan, X. Van der Waals integration before and beyond two-dimensional materials. *Nature* **2019**, *567*, 323−333.
(2) Jariwala, D.; Marks, T. J.; Hersam, M. C. Mixed-dimensional van der Waals heterostructures. *Nat. Mater.* **2017**, *16*, 170−181.
(3) Tan, C.; Cao, X.; Wu, X. J.; He, Q.; Yang, J.; Zhang, X.; Chen, J.; Zhao, W.; Han, S.; Nam, G. H.; Sindoro, M.; Zhang, H. Recent advances in ultrathin two-dimensional nanomaterials. *Chem. Rev.* **2017**, *117*, 6225−6331.
(4) Deng, X.-Z.; Zhang, J.-R.; Zhao, Y.-Q.; Yu, Z.-L.; Yang, J.-L.; Cai, M.-Q. The energy band engineering for the high-performance infrared photodetectors constructed by CdTe/MoS_2 heterojunction. *J. Phys.: Condens. Matter.* **2020**, *32*, No. 065004.
(5) Shao, Y.; Lv, W.; Guo, J.; Qi, B.; Lv, W.; Li, S.; Guo, G.; Zeng, Z. The current modulation of anomalous Hall effect in van der Waals Fe_3GeTe_2/WTe_2 heterostructures. *Appl. Phys. Lett.* **2020**, *116*, No. 092401.
(6) Liu, B.; Long, M.; Cai, M. Q.; Yang, J. L. Interface engineering of $CsPbI_3$-black phosphorus van der Waals heterostructure. *Appl. Phys. Lett.* **2018**, *112*, No. 043901.
(7) Li, Q.; Tang, L.; Zhang, C.; Wan, D.; Chen, Q. J.; Feng, Y. X.; Tang, L. M.; Chen, K. Q. Seeking the Dirac cones in the MoS_2/WSe_2 van der Waals heterostructure. *Appl. Phys. Lett.* **2017**, *111*, No. 171602.
(8) Krishnamoorthy, S.; Lee, E. W.; Lee, C. H.; Zhang, Y.; McCulloch, W. D.; Johnson, J. M.; Hwang, J.; Wu, Y.; Rajan, S. High current density 2D/3D MoS_2/GaN Esaki tunnel diodes. *Appl. Phys. Lett.* **2016**, *109*, No. 183505.
(9) Ruzmetov, D.; Zhang, K.; Stan, G.; Kalanyan, B.; Bhimanapati, G. R.; Eichfeld, S. M.; Burke, R. A.; Shah, P. B.; O'Regan, T. P.; Crowne, F. J.; Birdwell, A. G.; Robinson, J. A.; Davydov, A. V.; Ivanov, T. G. Vertical 2D/3D semiconductor heterostructures based on epitaxial molybdenum disulfide and gallium nitride. *ACS Nano* **2016**, *10*, 3580−3588.
(10) O'Regan, T. P.; Ruzmetov, D.; Neupane, M. R.; Burke, R. A.; Herzing, A. A.; Zhang, K.; Birdwell, A. G.; Taylor, D. E.; Byrd, E. F. C.; Walck, S. D.; Davydov, A. V.; Robinson, J. A.; Ivanov, T. G. Structural and electrical analysis of epitaxial 2D/3D vertical heterojunctions of monolayer MoS_2 on GaN. *Appl. Phys. Lett.* **2017**, *111*, No. 051602.
(11) Wan, Y.; Xiao, J.; Li, J.; Fang, X.; Zhang, K.; Fu, L.; Li, P.; Song, Z.; Zhang, H.; Wang, Y.; Zhao, M.; Lu, J.; Tang, N.; Ran, G.; Zhang, X.; Ye, Y.; Dai, L. Epitaxial single-layer MoS_2 on GaN with enhanced valley helicity. *Adv. Mater.* **2018**, *30*, No. 1703888.
(12) Chen, Z.; Liu, H.; Chen, X.; Chu, G.; Chu, S.; Zhang, H. Wafer-size and single-crystal $MoSe_2$ atomically thin films grown on GaN substrate for light emission and harvesting. *ACS Appl. Mater. Interfaces* **2016**, *8*, 20267−20273.
(13) Lee, E. W., II; Lee, C. H.; Paul, P. K.; Ma, L.; McCulloch, W. D.; Krishnamoorthy, S.; Wu, Y.; Arehart, A. R.; Rajan, S. Layer-transferred MoS_2/GaN PN diodes. *Appl. Phys. Lett.* **2015**, *107*, No. 103505.

(14) Su, M.; Chen, C.; Rajan, S. Prospects for the application of GaN power devices in hybrid electric vehicle drive systems. *Semicond. Sci. Technol.* **2013**, *28*, No. 074012.
(15) Ohno, Y.; Kuzuhara, M. Application of GaN-based heterojunction FETs for advanced wireless communication. *IEEE Trans. Electron Devices* **2001**, *48*, 517−523.
(16) Jellinek, F.; Brauer, G.; Muller, H. Molybdenum and niobium sulphides. *Nature* **1960**, *185*, 376−377.
(17) Murray, R.; Evans, B. The thermal expansion of 2H-MoS_2 and 2H-WSe_2 between 10 and 320 K. *J. Appl. Crystallogr.* **1979**, *12*, 312−315.
(18) Reeber, R. R.; Wang, K. Lattice parameters and thermal expansion of GaN. *J. Mater. Res.* **2000**, *15*, 40−44.
(19) Henck, H.; Aziza, Z. B.; Zill, O.; Pierucci, D.; Naylor, C. H.; Silly, M. G.; Gogneau, N.; Oehler, F.; Collin, S.; Brault, J.; Sirotti, F.; Bertran, F.; Fèvre, P. L.; Berciaud, S.; Johnson, A. T. C.; Lhuillier, E.; Rault, J. E.; Ouerghi, A. Interface dipole and band bending in the hybrid p-n heterojunction MoS_2/GaN (0001). *Phys. Rev. B* **2017**, *96*, No. 115312.
(20) Moun, M.; Kumar, M.; Garg, M.; Pathak, R.; Singh, R. Understanding of MoS_2/GaN heterojunction diode and its photodetection properties. *Sci. Rep.* **2018**, *8*, No. 11799.
(21) Tan, C.; Zhang, H. Two-dimensional transition metal dichalcogenide nanosheet-based composites. *Chem. Soc. Rev.* **2015**, *44*, 2713−2731.
(22) Tan, C.; Chen, J.; Wu, X. J.; Zhang, H. Epitaxial growth of hybrid nanostructures. *Nat. Rev. Mater.* **2018**, *3*, No. 17089.
(23) Zhang, Z.; Chen, P.; Duan, X. D.; Zang, K.; Luo, J.; Duan, X. Robust epitaxial growth of two-dimensional heterostructures, multiheterostructures, and superlattices. *Science* **2017**, *357*, 788−792.
(24) Kim, K. S.; Zhao, Y.; Jang, H.; Lee, S. Y.; Kim, J. M.; Kim, K. S.; Ahn, J. H.; Kim, P.; Choi, J. Y.; Hong, B. H. Large-scale pattern growth of graphene films for stretchable transparent electrodes. *Nature* **2009**, *457*, 706−710.
(25) Xie, S.; Tu, L.; Han, Y.; Huang, L.; Kang, K.; Lao, K. U.; Poddar, P.; Park, C.; Muller, D. A.; DiStasio, R. A., Jr.; Park, J. Coherent, atomically thin transition-metal dichalcogenide superlattices with engineered strain. *Science* **2018**, *359*, 1131−1136.
(26) Sahoo, P. K.; Memaran, S.; Xin, Y.; Balicas, L.; Gutiérrez, H. R. One-pot growth of two-dimensional lateral heterostructures via sequential edge-epitaxy. *Nature* **2018**, *553*, 63−67.
(27) Kang, K.; Xie, S.; Huang, L. J.; Han, Y. M.; Huang, P. Y.; Mak, K. F.; Kim, C. J.; Muller, D.; Park, J. High-mobility three-atom-thick semiconducting films with wafer-scale homogeneity. *Nature* **2015**, *520*, 656.
(28) Dudin, P.; Lacovig, P.; Fava, C.; Nicolini, E.; Bianco, A.; Cautero, G.; Barinov, A. Angle-resolved photoemission spectroscopy and imaging with a submicrometre probe at the SPECTROMICROSCOPY-3.2 L beamline of Elettra. *J. Synchrotron Radiat.* **2010**, *17*, 445−450.
(29) Yang, P.; Yang, A. G.; Chen, L.; Chen, J.; Zhang, Y.; Wang, H.; Hu, L.; Zhang, R. J.; Liu, R.; Qu, X. P.; Qiu, Z. J.; Cong, C. Influence of seeding promoters on the properties of CVD grown monolayer molybdenum disulfide. *Nano Res.* **2019**, *12*, 823−827.
(30) Ling, X.; Lee, Y. H.; Lin, Y. X.; Fang, W. J.; Yu, L. L.; Dresselhaus, M. S.; Kong, J. Role of the seeding promoter in MoS_2 growth by chemical vapor deposition. *Nano Lett.* **2014**, *14*, 464−472.
(31) Lee, Y. H.; Zhang, X. Q.; Zhang, W. J.; Chang, M. T.; Lin, C. T.; Chang, K. D.; Yu, Y. C.; Wang, J.; Chang, C. S.; Li, L. J.; Lin, T. W. Synthesis of large-area MoS_2 atomic layers with chemical vapor deposition. *Adv. Mater.* **2012**, *24*, 2320−2325.
(32) Zhang, S. C.; Kang, L. X.; Wang, X.; Tong, L. M.; Yang, L. W.; Wang, Z. Q.; Qi, K.; Deng, S. B.; Li, Q. W.; Bai, X. D.; Ding, F.; Zhang, J. Arrays of horizontal carbon nanotubes of controlled chirality grown using designed catalysts. *Nature* **2017**, *543*, 234−238.
(33) Radisavljevic, B.; Radenovic, A.; Brivio, J.; Giacometti, V.; Kis, A. Single-layer MoS_2 transistors. *Nat. Nanotechnol.* **2011**, *6*, 147−150.
(34) Ferrari, A. C.; Meyer, J. C.; Scardaci, V.; Casiraghi, C.; Lazzeri, M.; Mauri, F.; Piscanec, S.; Jiang, D.; K Novoselov, S.; Roth, S.; Geim, A. K. Raman spectrum of graphene and graphene layers. *Phys. Rev. Lett.* **2006**, *97*, No. 187401.
(35) Li, H.; Zhang, Q.; Yap, C. C. R.; Tay, B. K.; Edwin, T. H. T.; Olivier, A.; Baillargeat, D. From bulk to monolayer MoS_2: evolution of Raman scattering. *Adv. Funct. Mater.* **2012**, *22*, 1385−1390.
(36) Davydov, V. Y.; Kitaev, Y. E.; Goncharuk, I. N.; Smirnov, A. N.; Graul, J.; Semchinova, O.; Uffmann, D.; Smirnov, M. B.; Mirgorodsky, A. P.; Evarestov, R. A. Phonon dispersion and Raman scattering in hexagonal GaN and AlN. *Phys. Rev. B* **1998**, *58*, 12899−12907.
(37) Kuball, M. Raman spectroscopy of GaN, AlGaN and AlN for process and growth monitoring/control. *Surf. Interface Anal.* **2001**, *31*, 987−999.
(38) Taube, A.; Judek, J.; Łapińska, A.; Zdrojek, M. Temperature-dependent thermal properties of supported MoS_2 monolayers. *ACS Appl. Mater. Interfaces* **2015**, *7*, 5061−5065.
(39) Yan, R.; Simpson, J. R.; Bertolazzi, S.; Brivio, J.; Watson, M.; Wu, X.; Kis, A.; Luo, T.; Hight Walker, A. R.; Xing, H. G. Thermal conductivity of monolayer molybdenum disulfide obtained from temperature-dependent Raman spectroscopy. *ACS Nano* **2014**, *8*, 986−993.
(40) Zhang, X.; Qiao, X. F.; Shi, W.; Wu, J. B.; Jiang, D. S.; Tan, P. H. Phonon and Raman scattering of two-dimensional transition metal dichalcogenides from monolayer, multilayer to bulk material. *Chem. Soc. Rev.* **2015**, *44*, 2757−2785.
(41) Mak, K. F.; Lee, C.; Hone, J.; Shan, J.; Heinz, T. F. Atomically thin MoS_2: A new direct-gap semiconductor. *Phys. Rev. Lett.* **2010**, *105*, No. 136805.
(42) McCreary, K. M.; Hanbicki, A. T.; Sivaram, S. V.; Jonker, B. T. A-and B-exciton photoluminescence intensity ratio as a measure of sample quality for transition metal dichalcogenide monolayers. *APL Mater.* **2018**, *6*, No. 111106.
(43) Yang, P.; Shan, Y.; Chen, J.; Ekoya, G.; Han, J.; Qiu, Z. J.; Sun, J.; Chen, F.; Wang, H.; Bao, W.; Hu, L.; Zhang, R. J.; Liu, R.; Cong, C. Remarkable quality improvement of as-grown monolayer MoS_2 by sulfur vapor pretreatment of SiO_2/Si substrates. *Nanoscale* **2020**, *12*, 1958.
(44) Jeong, H.; Oh, H. M.; Gokarna, A.; Kim, H.; Yun, S. J.; Han, G. H.; Jeong, M. S.; Lee, Y. H.; Lerondel, G. Integrated freestanding twos-dimensional transition metal dichalcogenides. *Adv. Mater.* **2017**, *29*, No. 1700308.
(45) Wan, Y.; Zhang, H.; Wang, W.; Sheng, B.; Zhang, K.; Wang, Y.; Song, Q.; Mao, N.; Li, Y.; Wang, X.; Zhang, J.; Dai, L. Origin of improved optical quality of monolayer molybdenum disulfide grown on hexagonal boron nitride substrate. *Small* **2016**, *12*, 198−203.
(46) Zhou, D.; Shu, H.; Hu, C.; Jiang, L.; Liang, P.; Chen, X. Unveiling the growth mechanism of MoS_2 with chemical vapor deposition: from two-dimensional planar nucleation to self-seeding nucleation. *Cryst. Growth Des.* **2018**, *18*, 1012−1019.
(47) Kim, I. S.; Sangwan, V. K.; Jariwala, D.; Wood, J. D.; Park, S.; Chen, K. S.; Shi, F. Y.; Ruiz-Zepeda, F.; Ponce, A.; Jose-Yacaman, M.; Dravid, V. P.; Marks, T. J.; Hersam, M. C.; Lauhon, L. J. Influence of stoichiometry on the optical and electrical properties of chemical vapor deposition derived MoS_2. *ACS Nano* **2014**, *8*, 10551−10558.
(48) Carin, R.; Deville, J. P.; Werckmann, J. An XPS study of GaN thin films on GaAs. *Surf. Interface Anal.* **1990**, *16*, 65−69.
(49) Avila, J.; Razado-Colambo, I.; Lorcy, S.; Lagarde, B.; Giorgetta, J.-L.; Polack, F.; Asensio, M. C. ANTARES, a scanning photoemission microscopy beamline at SOLEIL. *J. Phys.: Conf. Ser.* **2013**, *425*, No. 192023.
(50) Yang, H.; Liang, A.; Chen, C.; Zhang, C.; Schroeter, N. B. M.; Chen, Y. Visualizing electronic structures of quantum materials by angle-resolved photoemission spectroscopy. *Nat. Rev. Mater.* **2018**, *3*, 341−353.
(51) Yuan, H.; Liu, Z.; Xu, G.; Zhou, B.; Wu, S.; Dumcenco, D.; Yan, K.; Zhang, Y.; Mo, S.-K.; Dudin, P.; Kandyba, V.; Yablonskikh, M.; Barinov, A.; Shen, Z.; Zhang, S.; Huang, Y.; Xu, X.; Hussain, Z.; Hwang, H. Y.; Cui, Y.; Chen, Y. Evolution of the valley position in bulk transition-metal chalcogenides and their monolayer limit. *Nano Lett.* **2016**, *16*, 4738.

https://doi.org/10.1021/acsanm.1c02662
ACS Appl. Nano Mater. 2021, 4, 12127−12136

(52) Jin, W.; Yeh, P. C.; Zaki, N.; Zhang, D.; Sadowski, J. T.; AlMahboob, A.; van der Zande, A. M.; Chenet, D. A.; Dadap, J. I.; Herman, I. P.; Sutter, P.; Hone, J.; Osgood, R. M. Direct measurement of the thickness-dependent electronic band structure of MoS_2 using angle-resolved photoemission spectroscopy. *Phys. Rev. Lett.* **2013**, *111*, No. 106801.
(53) Jain, S. K.; Kumar, R. R.; Aggarwal, N.; Vashishtha, P.; Goswami, L.; Kuriakose, S.; Pandey, A.; Bhaskaran, M.; Walia, S.; Gupta, G. Current transport and band alignment study of MoS_2/GaN and MoS_2/AlGaN heterointerfaces for broadband photodetection application. *ACS Appl. Electron. Mater.* **2020**, *2*, 710−718.
(54) Jain, S. K.; Low, M. X.; Taylor, P. D.; Tawfik, S. A.; Spencer, M. J. S.; Kuriakose, S.; Arash, A.; Xu, C.; Sriram, S.; Gupta, G.; Bhaskaran, M.; Walia, S. 2D/3D hybrid of MoS_2/GaN for a high -performance broadband photodetector. *ACS Appl. Electron. Mater.* **2021**, *3*, 2407−2414.
(55) Lopez-Sanchez, O.; Lembke, D.; Kayci, M.; Radenovic, A.; Kis, A. Ultrasensitive photodetectors based on monolayer MoS_2. *Nat. Nanotechnol.* **2013**, *8*, 497−501.
(56) Krishnamurthi, V.; Low, M. X.; Kuriakose, S.; Sriram, S.; Bhaskaran, M.; Walia, S. Black phosphorus nanoflakes vertically stacked on MoS_2 nanoflakes as heterostructures for photodetection. *ACS Appl. Nano Mater.* **2021**, *4*, 6928−6935.

https://doi.org/10.1021/acsanm.1c02662
ACS Appl. Nano Mater. 2021, 4, 12127−12136